Microscale Localized Spectroscopy with a Magnetic Resonance Force Microscope

C. L. Degen, Q. Lin, A. Hunkeler, U. Meier, M. Tomaselli, and B. H. Meier*

Physical Chemistry, ETH Zurich, CH-8093 Zurich, Switzerland.

(Received 28 January 2005; published 26 May 2005)

Magnetic resonance force microscopy is combined with spin-echo spectroscopy to obtain spatially and spectrally resolved NMR signals of micrometer-scale objects. The experimental spatial resolution for the demonstration experiment on a sample consisting of $Ba(ClO_3)_2 \cdot H_2O$ and $(NH_4)_2SO_4$ single crystals is 3.4 μm. The spectral resolution of 3.4 kHz is sample limited. Improvements in resolution and extensions of the method to more than one spatial dimension and to multidimensional spectroscopy are possible.

DOI: 10.1103/PhysRevLett.94.207601 PACS numbers: 76.60.Lz, 76.60.Pc

Nuclear magnetic resonance (NMR) and magnetic resonance imaging (MRI) are powerful structural diagnostics and imaging tools in medicine, biology, chemistry, material sciences, and physics [1]. NMR investigates the local spin interactions of the sample in a homogeneous magnetic field and allows molecular structure determination with Ångstrom precision. MRI introduces (pulsed) magnetic field gradients to record a spatial image of the spin density. Localized spectroscopy combines spatial and spectral dimensions to obtain the NMR spectrum for each volume element of the sample and adds superb chemical contrast to imaging. The work described in the following extends local spectroscopy of spin-1/2 nuclei in solids to the micrometer scale.

The applicability of NMR and MRI to microscale samples is restricted by the low sensitivity of the conventional Faraday detection method and the availability of strong magnetic field gradients. An alternative approach to observe the polarization from a small number of spins, down to a single electron spin [2], measures the magnetic moment as a force exerted on the sample in a magnetic field gradient. Sidles and co-workers [3,4] coined this concept into the magnetic resonance force microscope (MRFM) constituting a promising next-generation magnetic resonance detection device. In MRFM the sample or a small magnet attached to a micromechanical oscillator is driven by a cyclic modulation of the spin magnetization at resonance by suitable radio-frequency (rf) irradiation schemes. In addition to a gain in sensitivity, the large inhomogeneous field produced by the gradient magnet up to values exceeding 10^5 T/m allows us to perform magnetic resonance imaging with submicron spatial resolution even in the presence of broad resonance lines [2,5].

The large field gradient is, however, detrimental for high-resolution magnetic resonance applications [6]. Several strategies have been presented to circumvent this problem: force detection in a homogeneous field has been demonstrated for electron paramagnetic resonance by measuring the mechanical torque on a sample by transfer of spin angular momentum [7]. Another approach is the Boomerang experiment [8], where a carefully selected assembly of ferromagnetic elements allows for a homogeneous field at the sample position, yet it is still possible to produce a net force on the mechanical oscillator. For exploring quadrupolar nuclei, MRFM-detected nutation spectroscopy has been introduced [9].

In this Letter we describe the recording of gradient-free NMR spectra with the unprecedented imaging resolution of magnetic resonance force microscopy. The approach presented is applicable if the NMR spectrum is dominated by spin-spin (homonuclear and heteronuclear dipole and J couplings) or quadrupole interactions. In this case, a Hahn spin echo in the indirectly sampled spectral dimension exclusively refocuses the effect of the static field gradient [10–13]. The method is related to the work of Verhagen on quadrupolar nuclei [9] and is, in some respects, reminiscent of separated-local field spectroscopy [14]. In the following, we concentrate on spin-1/2 ensembles whose spectral line shape is dominated by dipole interactions among like spins as often encountered for high-γ nuclei in solids.

MRFM spin-echo experiments have been performed on a $Ba(ClO_3)_2 \cdot H_2O$ single crystal, where the two protons within a water molecule give rise to a distinct doublet with an orientation dependent splitting of $\omega_d/2\pi = 44 \times (3\cos^2\beta - 1)$ kHz [15,16]. The measured coherence decay in the local field and the associated spectrum are shown in Fig. 1. The gradient-broadened decay [or free induction decay (FID in Fig. 1)] and spectrum in the absence of the echo pulse are also displayed. This spectrum reflects the width of the sensitive slice (200 kHz) for detection and is almost 2 orders of magnitude wider than the sharp dipole lines of ~3.4 kHz easily distinguished in the echo spectrum. A comparison of the echo spectrum with the conventional inductive NMR spectrum recorded at 220 MHz and with the calculated second moment according to the crystal structure suggests that the residual line broadening is intrinsic rather than caused by an incomplete refocusing of the gradient inhomogeneity.

Figures 2(a) and 2(b) depict the applied rf protocol. During the evolution period t_1, the spin coherence prepared by the first $\pi/2$ pulse evolves under the influence of all

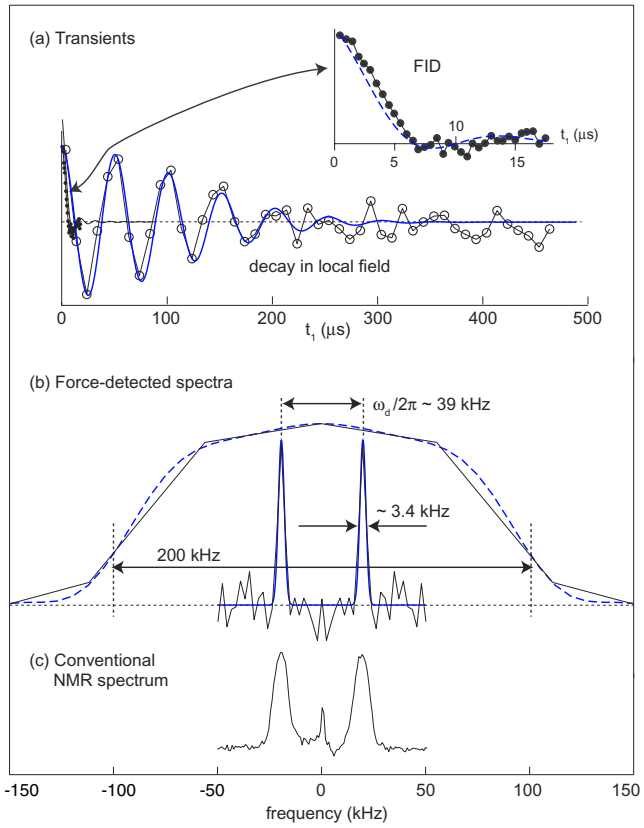

FIG. 1 (color online). (a) MRFM-detected coherence decay of $\sim 10^{14}$ proton spins in a $Ba(ClO_3)_2 \cdot H_2O$ single crystal with and without a Hahn spin echo (2 transients, total experimental time 50 min), using the rf scheme described in Fig. 2. Only the real part of the complex magnetization was measured [27]. The solid line corresponds to a fit with a cosine of 19.6 kHz multiplied by a Gaussian decay ($\sigma = 111$ μs). (b) Experimental spectra obtained by a Fourier transform. The gradient-broadened result is well explained by a simulation [dashed lines in (a) and (b)] that takes finite pulse lengths and the efficiency of cantilever excitation by the applied magnetization modulation scheme into account. The experimental spectrum employing the Hahn echo shows a clearly resolved dipolar splitting. The best fit by a Gaussian line is shown by a solid line. (c) NMR result of a mm-sized single crystal at an orientation which produces the same dipolar line splitting. The broader linewidth, compared with (b), can be caused by a different crystal orientation (polar angle φ) and/or a mosaic disorder of the large crystal.

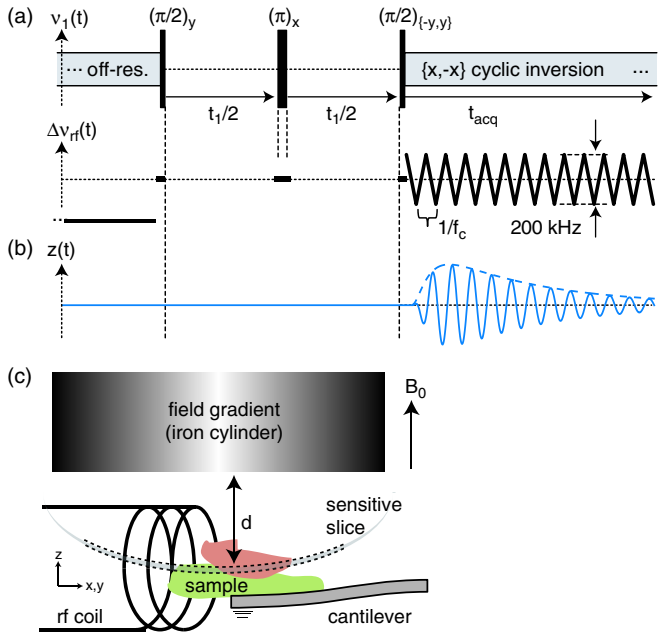

FIG. 2 (color online). (a) Pulse-timing diagram employed in our experiments. Pulses are given as $(\text{flip angle})_{\text{phase}}$. rf-field strengths were $\omega_1/2\pi \sim 210$ kHz (1.2 μs $\pi/2$ pulse width) and ~ 15 kHz for pulsing and cyclic adiabatic inversion, respectively. A 0.5 s off-resonance (-400 kHz) irradiation prior to the experiment and a two-step phase cycle (indicated by {}) eliminated spurious rf-cantilever couplings. The repetition delay between scans was 30 s [28]. The triangular frequency modulation used for cyclic adiabatic inversion had a depth of 200 kHz in all experiments, and its rate matched the cantilever eigenfrequency of typically 850 Hz. (b) Schematic drawing of the cantilever oscillations and the detected output of the lock-in amplifier (dashed line), which is then integrated over $t_{\text{acq}} = 3$ s. (c) Experimental setup. A cylindrical iron magnet ($B_{\text{sat}} \sim 1.75$ T) of 1 mm diameter ($\ll$ length) produced approximately planar surfaces of constant field (sensitive slices, dashed shape) perpendicular to the static field axis ($B_0 = 5.9$ T, 250 MHz proton frequency). The field gradient at $d = 200$ μm was $\partial B_z/\partial z \sim 1'400$ T/m. Typical cantilever parameters were $k = 17$ mN/m, $f_c = 850$ Hz and $Q = 10'000$ ($Q_{\text{cl}} = 20$ with feedback). The 4 turn, 200 μm inner diameter coil was wound from 50 μm thick copper wire.

terms of the internal spin Hamiltonian [17] and of the external field gradient. A second $\pi/2$ pulse at the end of the evolution period converts the spin coherence back to M_z magnetization, which is adiabatically modulated during t_{acq} for MRFM readout. The spin-echo π pulse, when applied exactly at $t_1/2$, selectively refocuses the effect of the external field gradient [13]. Because the MRFM readout samples the echo peak amplitude for a series of t_1 a dipolar spectrum free of inhomogeneity broadening is obtained after Fourier transform with respect to t_1.

Our MRFM setup [Fig. 2(c)] follows the sample-on-cantilever design [4] and operates inside a standard wide-bore NMR magnet at room temperature and under vacuum conditions ($p < 10^{-5}$ mbar) [18]. The sample was glued with epoxy onto the cantilever tip (Veeco Instruments) and brought near a gradient magnet much larger in size. Motions were sensed by means of a deflected laser beam [19] and analyzed by a lock-in amplifier (SR830, Stanford Research). Feedback control applied to a piezo attached to the lever's base increased the bandwidth and kept the damping time acceptably low [20]. A broadband, impedance matched rf circuit incorporating a solenoid coil produced the necessary field for pulsing and frequency

modulation. rf pulses were prepared by an arbitrary waveform generator (NI-5411, National Instruments) followed by a power amplifier stage (Blax1000, Bruker BioSpin) [21]. A "gradient lock" was implemented in order to compensate for long-term drifts of the Larmor frequency, caused by mechanical instabilities of the gradient source positioning and temperature variations [22].

Spatially resolved force spectroscopy is demonstrated on a phantom consisting of a pair of single crystals of $(NH_4)_2SO_4$ and $Ba(ClO_3)_2 \cdot H_2O$, respectively. In contrast to $Ba(ClO_3)_2 \cdot H_2O$, the 30 kHz wide spectrum of $(NH_4)_2SO_4$ is featureless (see below). A one-dimensional (1D) MRFM image of the phantom along the z axis is shown on the left side of Fig. 3. Spatial coordinates were inferred from the Larmor frequency and the calculated field distribution of the gradient magnet. Localized spectroscopy was performed at different positions of the phantom, resulting in the echo decay curves and the corresponding dipolar spectra plotted on the right. Three regions can be identified: In **A**, only $(NH_4)_2SO_4$ is present. The spectrum shows a single broad line in accordance with the conventional NMR spectrum (not shown). Region **C** consists of only $Ba(ClO_3)_2 \cdot H_2O$ with a doublet splitting of $\sim$19.5 kHz. The splitting differs from the one in Fig. 1 due to the different crystal orientation. **B** represents the intermediate region, where both $(NH_4)_2SO_4$ and $Ba(ClO_3)_2 \cdot H_2O$ are present. Spectrum **B** can be reconstructed as a linear superposition of **A** and **C**, indicated by the dashed spectrum.

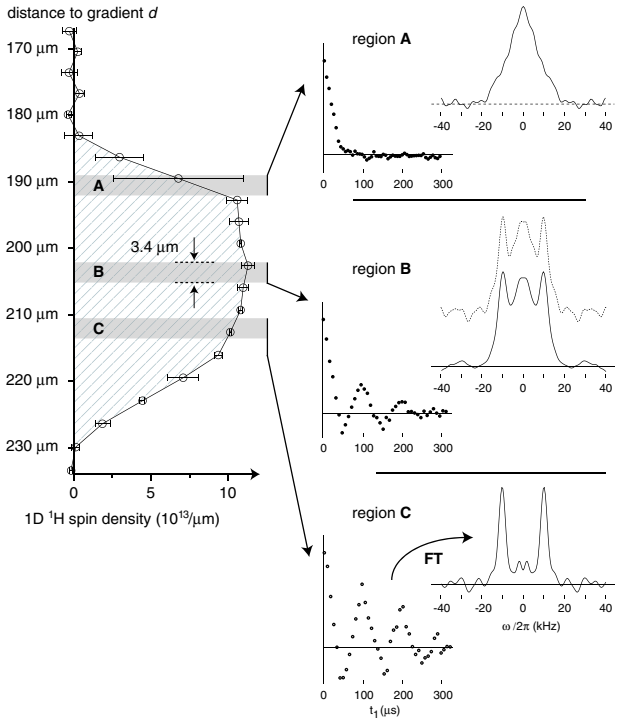

FIG. 3 (color online). Left: 1D ^{1}H spin-density image along the z axis of a sample consisting of a $(NH_4)_2SO_4$ and a $Ba(ClO_3)_2 \cdot H_2O$ single crystal, mounted side-by-side on the MRFM cantilever. Sample thickness was $\sim$35 μm and lateral dimensions $\sim 90 \times 110 \mu m^2$, determined by an optical microscope. Error bars are estimated from the difference to a subsequent control measurement. The high uncertainty at the sharp upper edge can be attributed to the positional inaccuracy [22]. The spin-density scale is calibrated within a factor of $\sim$1.4 as described in Fig. 4. Right: Local spectra at three different locations (4 transients each) as described in the text.

The knowledge of the pure substance spectra allows us to filter the spatial image with respect to the components. A general scheme requires a spectrum at each spatial position and yields a spin-density profile for each constituent (provided the spectra are not too similar). In the present simple case, however, we take advantage of the different spin-echo decay curves: for $t_1 \sim 54$ μs, the $(NH_4)_2SO_4$ signal has completely dephased, while $Ba(ClO_3)_2 \cdot H_2O$ exhibits a negative signal with $\sim$35% of the total intensity [cf. Figure 3, right side]. An image recorded with this filter is added on the left side of Fig. 4. The spin-density distribution for each substance (shown on the right) is easily reconstructed by linear combination.

We have shown that—in spite of the large field gradient—localized dipolar NMR spectroscopy is readily implemented in magnetic resonance force microscopy. The resulting spin-echo spectra have been used to obtain concentration profiles of the constituent substances. The spatial resolution is limited by the size of the field gradient and detection sensitivity only and is no different than in

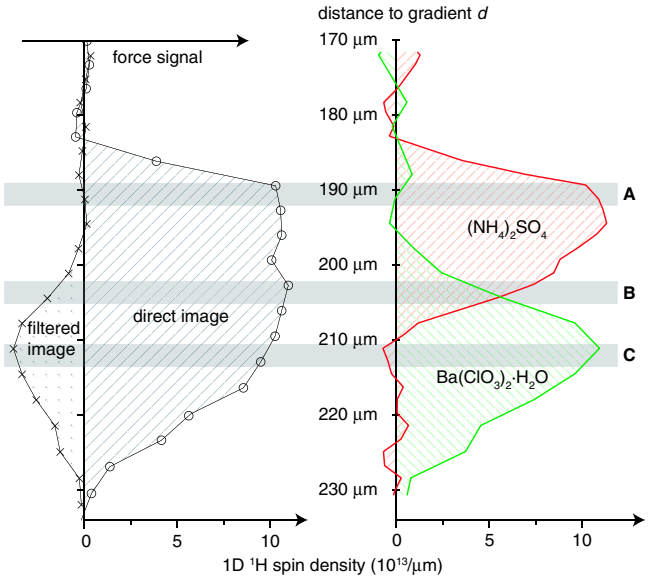

FIG. 4 (color online). Direct and echo filtered image of the phantom (left), and chemically selective image of $(NH_4)_2SO_4$ and $Ba(ClO_3)_2 \cdot H_2O$ (right). The approximate ^{1}H spin density, proportional to the integrated intensity [29], was calibrated by the sample's mass (inferred from the motional mass of the cantilever) and the filtered image of $Ba(ClO_3)_2 \cdot H_2O$. The estimated absolute calibration in the spin-density scale is determined to within a factor of $\sim$1.4.

other MRFM experiments. In our case, however, on the order of 100 data points in the spectral domain must be recorded, increasing the measuring time and putting demands on the long-time stability of the measurement setup. The spectral resolution observed is sample limited.

Although this work concentrates on dipolar couplings, the presented MRFM technique can be extended using more sophisticated rf-preparation schemes. Heteronuclear dipolar and J couplings can be studied by applying selective double-resonant rf pulses [23,24]. High-resolution chemical-shift information can possibly be restored by zero-quantum and total-coherence spectroscopy [25,26]. Using the inherent imaging capacity of MRFM, we plan to extend localized spectroscopy with these methods to obtain spatially resolved spectroscopic information and chemical contrast on a wide class of microstructured and nanostructured materials.

The authors are grateful to A. Kentgens, A. Baumgartner, K. Ensslin, E. Meyer, H. Schniepp, and V. Sandoghdar for their advice during the construction of the MRFM apparatus. We thank the ETH Zurich, the Schweizerischer Nationalfonds (SNF), and the Kommission für Technologie und Innovation (KTI) for financial support.

*Electronic address: beme@ethz.ch

[1] R. R. Ernst, Angew. Chem., Int. Ed. Engl. **31**, 805 (1992); K. Wüthrich, J. Biomol. NMR **27**, 13 (2003); P. Mansfield, Angew. Chem., Int. Ed. Engl. **43**, 5456 (2004).

[2] D. Rugar, R. Budakian, H. J. Mamin, and B. W. Chui, Nature (London) **430**, 329 (2004).

[3] J. A. Sidles, Appl. Phys. Lett. **58**, 2854 (1991).

[4] D. Rugar, O. Züger, S. Hoen, C. S. Yannoni, H.-M. Vieth, and R. D. Kendrick, Science **264**, 1560 (1994).

[5] O. Züger and D. Rugar, Appl. Phys. Lett. **63**, 2496 (1993).

[6] A similar problem is encountered in conventional stray-field imaging; for a review see P. J. McDonald and B. Newling, Rep. Prog. Phys. **61**, 1441 (1998).

[7] G. Alzetta, E. Arimondo, C. Ascoli, and A. Gozzini, Nuovo Cimento B **52**, 392 (1967); C. Ascoli, P. Baschieri, C. Frediani, L. Lenci, M. Martinelli, G. Alzetta, R. M. Celli, and L. Pardi, Appl. Phys. Lett. **69**, 3920 (1996).

[8] G. M. Leskowitz, L. A. Madsen, and D. P. Weitekamp, Solid State Nucl. Magn. Reson. **11**, 73 (1998); L. A. Madsen, G. M. Leskowitz, and D. P. Weitekamp, Proc. Natl. Acad. Sci. U.S.A. **101**, 12804 (2004).

[9] R. Verhagen, A. Wittlin, C. W. Hilbers, H. van Kempen, and A. P. M. Kentgens, J. Am. Chem. Soc. **124**, 1588 (2002).

[10] E. L. Hahn, Phys. Rev. **80**, 580 (1950).

[11] K. Wago, D. Botkin, C. S. Yannoni, and D. Rugar, Phys. Rev. B **57**, 1108 (1998).

[12] O. Klein, V. V. Naletov, and H. Alloul, Eur. Phys. J. B **17**, 57 (2000).

[13] The dipolar evolution, or any even-order spin interaction, is unaffected as long as the coupling between spins is considerably larger than their resonance frequency differences (induced by differences in the chemical shift or extremely strong gradients). For a spin $I > 1/2$ all odd rank tensor components of the quadrupole Hamiltonian are generally refocused.

[14] R. K. Hester, J. L. Ackerman, B. L. Neff, and J. S. Waugh, Phys. Rev. Lett. **36**, 1081 (1976); E. F. Rybaczewski, B. L. Neff, J. S. Waugh, and J. S. Sherfinski, J. Chem. Phys. **67**, 1231 (1977).

[15] β denotes the angle between the internuclear vector and $\mathbf{B_0}$.

[16] R. D. Spence, J. Chem. Phys. **23**, 1166 (1955); J. W. McGrath and A. A. Silvidi, J. Chem. Phys. **34**, 322 (1961).

[17] R. R. Ernst, G. Bodenhausen, and A. Wokaun, *Principles of Nuclear Magnetic Resonance in One and Two Dimensions* (Clarendon, Oxford, 1987).

[18] Q. Lin *et al.*, (unpublished).

[19] G. Meyer and N. M. Amer, Appl. Phys. Lett. **53**, 2400 (1988).

[20] C. L. Degen, U. Meier, Q. Lin, A. Hunkeler, and B. H. Meier, (unpublished).

[21] R. Verhagen, C. W. Hilbers, A. P. M. Kentgens, L. Lenci, R. Groeneveld, A. Wittlin, and H. van Kempen, Phys. Chem. Chem. Phys. **1**, 4025 (1999).

[22] A "snapshot" MRFM image of the sample under investigation was recorded in fixed time intervals (i.e., every 20 min). The median of such an image defined the sample's center Larmor frequency, which was fed into a linear predictor and continuously updated. The Larmor frequencies (and thus, the spatial positions) of all sensitive slices were then referred relative to the sample center frequency, resulting in a relative positional accuracy of ca. ± 50 kHz (± 1 μm).

[23] D. E. Kaplan and E. L. Hahn, J. Phys. Radium **19**, 821 (1958).

[24] A. Pines, M. S. Gibby, and J. S. Waugh, J. Chem. Phys. **59**, 569 (1973).

[25] A. Wokaun and R. R. Ernst, Chem. Phys. Lett. **52**, 407 (1977).

[26] D. P. Weitekamp, J. R. Garbow, J. B. Murdoch, and A. Pines, J. Am. Chem. Soc. **103**, 3578 (1981); J. R. Garbow, D. P. Weitekamp, and A. Pines, J. Chem. Phys. **79**, 5301 (1983).

[27] A complex spectrum could be recorded by time proportional phase incrementing the last $\pi/2$ pulse. See Ref. [17], p. 340.

[28] Experimental spin-lattice relaxation times T_1 were 4.1 and 8.9 s for $(NH_4)_2SO_4$ and $Ba(ClO_3)_2 \cdot H_2O$, respectively.

[29] The integrated signal intensity is proportional to $T_{1\rho}^{\mathrm{MRFM}} \cdot M_z$, where the magnetization $M_z \propto$ number of spins. The experimentally determined relaxation time under cyclic adiabatic inversion was the same for both components, $T_{1\rho}^{\mathrm{MRFM}} \sim 1.5$ s.